Appl. Math. Mech. -Engl. Ed., **45**(3), 441–460 (2024)

APPLIED MATHEMATICS AND MECHANICS (ENGLISH EDITION)

https://doi.org/10.1007/s10483-024-3097-7

Dynamic analysis of axle box bearings on the high-speed train caused by wheel-rail excitation*

Qiaoying MA[1,2], Shaopu YANG[1], Yongqiang LIU[1,3,†], Baosen WANG[1,3], Zechao LIU[1]

1. State Key Laboratory of Mechanical behavior and System Safety of Traffic Engineering Structures, Shijiazhuang Tiedao University, Shijiazhuang 050043, China;
2. School of Transportation, Shijiazhuang Tiedao University, Shijiazhuang 050043, China;
3. School of Mechanical Engineering, Shijiazhuang Tiedao University, Shijiazhuang 050043, China

(Received Dec. 11, 2023 / Revised Jan. 21, 2024)

Abstract To explore the impact of wheel-rail excitation on the dynamic performance of axle box bearings, a dynamic model of the high-speed train including axle box bearings is developed. Subsequently, the dynamic response characteristics of the axle box bearing are examined. The investigation focuses on the acceleration characteristics of bearing vibration under excitation of track irregularities and wheel flats. In addition, experiments on both normal and faulty bearings are conducted separately, and the correctness of the model and some conclusions are verified. According to the research, track irregularity is unfavorable for bearing fault detection based on resonance demodulation. Under the same speed conditions, the acceleration peak of bearing is inversely proportional to the length of the wheel flat and directly proportional to its depth. The paper will contribute to a deeper understanding of the dynamic performance of axle box bearings.

Key words high-speed train, track irregularity, wheel flat, dynamic simulation

Chinese Library Classification O357
2010 Mathematics Subject Classification 74A05, 74H15

1 Introduction

Wheel-rail excitation is a hot topic in the research of high-speed railway vehicles. Xu and Yu[1], for example, studied the relationship between wheels and rails. Liang et al.[2] simulated

* Citation: MA, Q. Y., YANG, S. P., LIU, Y. Q., WANG, B. S., and LIU, Z. C. Dynamic analysis of axle box bearings on the high-speed train caused by wheel-rail excitation. *Applied Mathematics and Mechanics* (*English Edition*), **45**(3), 441–460 (2024) https://doi.org/10.1007/s10483-024-3097-7

† Corresponding author, E-mail: liuyq@stdu.edu.com

Project supported by the National Natural Science Foundation of China (Nos. 12393780, 12032017, and 12002221), the Key Scientific Research Projects of China Railway Group (No. N2021J032), the College Education Scientific Research Project in Hebei Province of China (No. JZX2024006), the S&T Program in Hebei of China (No. 21567622H), and the Research Project of Hebei Province Science and Technology (No. QN2023071)

the track irregularity excitation and theoretically studied the dynamic interaction of the vehicle-track-subgrade system. However, the wheelset may be damaged after long-term operation, which will cause more serious wheel-rail disturbances, such as wheel flat. It is a kind of tread scratch that will affect the rolling roundness of the wheel and form periodic pulse excitation between wheel and rail. The impact load resulting from a wheel flat defect is huge and will directly affect the operation of the wheel axle. As the inner ring of the bearing is directly installed on the axle, the periodic shock caused by wheel flats may increase significantly under its high-speed rotation, which will seriously endanger the safety of the bearing and lead to more serious accidents. Consequently, It is highly relevant and practical to delve into the dynamic issues of bearings triggered by wheel-rail excitation.

In recent years, many experts and scholars have explored and researched the wheel-rail contact relationship under the impact of wheel flats. Regarding the issue of train wheelset slipping, Yin et al.[3] suggested a technique for early slipping fault detection that can achieve millisecond-level detection of slipping defects. Han et al.[4–5] established the wheel flat in a three-dimensional (3D) wheel-rail rolling model. The dynamic finite element simulation was conducted. It can be found that there will be a significant wheel-rail dynamic impact force generated by the wheel flat, and it is much greater than the static axle load. Meanwhile, the axle load, flat length, and train speed all had an impact on the wheel-rail[6]. Steenbergen[7] developed the speed criterion considering the contact loss of wheel-rail, and studied the characteristics of the flat in the subcritical speed regime and in the transcritical speed. Liu et al.[8] discussed the precaution, geometric representation, physical attributes, and reason for flat damage on wheels. Bian et al.[9] created a 3D finite element model of wheel-rail contact and investigated the dynamic response of wheel-rail impacts caused by wheel flats. Besides, Bian et al.[10] studied the effects of the wheel flat on the impact force under a critical wheel flat size. Qin et al.[11] looked into the evolution law of wheel-rail response when one or two flat defects are present on the wheel and determined the allowable limit of flats on the wheel tread. Dukkipati and Dong[12] investigated the characteristics of impact loads resulting from wheel flats using the vehicle-track system finite element mode. It has been discovered that the vehicle speed and the size and form of the wheel flat are the primary factors influencing the impact load.

The above scholars have studied the vehicle dynamic response under the wheel flat; meanwhile, some scholars have done research on bearings. Using the proposed model, Zhao et al.[13] investigated the dynamic interaction between the cage and rollers of bearings and validated the importance of flexibility and pocket clearance. Lu et al.[14] developed an axle box bearing model with multitype faults and vehicle systems, and performed a theoretical analysis of rolling tracks that go through the damage locations. Li et al.[15] created a coupling model of gear-rotor-bearing system，and systematically studied the system's vibration response by adjusting the bearing clearance, speed, and eccentricity. Liu and Shao[16] established a new type bearing dynamic model, taking into account the lubricating oil film and time-varying excitation of contact stiffness, and the vibration response of bearings with surface waviness defects was examined. Liu and Shao[17] further proposed a revised analytical model that takes lubrication into account for roller bearings. The relationship between vibration impulses and localized defects with different edge shapes was analyzed. For a high-speed train running at variable speeds, Wang et al.[18] and Liu et al.[19] created a dynamic model of the axle box bearing and rotor system. They further analyzed the temperature and lubrication characteristics of the bearing using the original model and focused on the effects of bearing faults on system stability. Tian et al.[20] built a dynamic model for bearing and studied the dynamic properties of it with localized defects, which are subject to time-varying displacement excitation. Hou et al.[21] investigated the dynamic contact load distribution of gearbox bearings on the high-speed train, established the bearing outer ring's most load position, and thoroughly investigated the characteristics and causes of load variations.

However, considering that the axle box bearing's motion is intimately associated with the

operating environment of the vehicle, its vibration may also be affected by the wheel flat. In this case, some scholars have carried out a dynamic analysis of train bearings under external excitation factors. Studies of Liu et al.[22–23] showed that the random irregularity of the track in conjunction with the wheel-rail would worsen the motor bearings' operational conditions. Besides, it was concluded that through the internal excitation and external excitation, the vibration acceleration of the motor and its adjacent components of the vehicle increases with the amplitude of the bearing surface waviness. Li et al.[24] developed a spatially coupled dynamic model of the vehicle-track. The study demonstrated that there is a strong nonlinear coupled relationship between the axle box vibration and the vehicle. The effects of the roundness and waviness errors of the bearing on the vibrations of vehicle were studied, and the superiority of the proposed model was proved in Refs. [25]–[27]. In addition, some scholars have carried out dynamic analyses of axle box bearings separately[28–29].

Through the above review, it can be found that the vibration of the bearing will be affected by external excitation factors. Connecting the bearing with the actual running environment of the vehicle can more truly reflect its operating conditions. However, in the present research, the analysis of the bearing dynamics under the wheel-rail excitation is still very lacking, and so is the vibration law of the axle box bearing. Therefore, with the axle box bearing model in the vehicle, this paper conducts a dynamic analysis of the axle box bearing under the influence of wheel-rail excitation. The objective is to clarify the axle box bearing's vibration law under wheel-rail excitation and to establish a foundation for the examination of bearing performance degradation.

2 Modeling of axle box bearings included in the vehicle

2.1 Vehicle model

The vehicle model is established through universal mechanism (UM), which is a multi-body dynamics simulation software. The vehicle model consists of a car body (6 degrees of freedom), 2 bogies (6 degrees of freedom), 4 wheel pairs (6 degrees of freedom), 8 axle boxes (3 degrees of freedom), and primary and secondary suspensions, as shown in Fig. 1. The vehicle model's specifications are based on the 380B rolling stock, and its main parameters can be found in Ref. [30]. The calculation of the wheel-rail contact force is a major difficulty in the calculation of vehicle models. In the calculation process of the model, the wheel-rail contact algorithm uses FASTSIM, a fast calculation model, and the simplified theory of the Kalker algorithm to solve the model in the paper. It can be used to simulate the behavior of wheel-rail contact and compute responses like displacement or stress at the contact points.

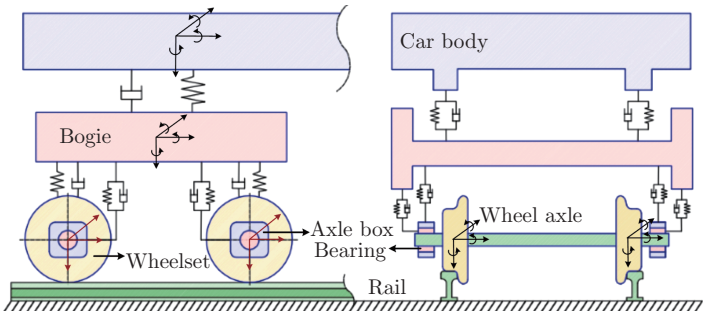

Fig. 1 Model structure diagram (color online)

2.2 Axle box bearing model

The axle box bearings (translational freedom in the X-, Y-, and Z-directions) are double-row tapered roller bearing, consisting of the inner ring, the outer ring, and roller elements. It

is established by the MATLAB/SIMULINK module. In the modeling process, the components of the vehicle model and the axle box bearing model are regarded as rigid bodies, and their elastic deformation is not considered. Among them, due to the complex structure of the axle box bearing, some simplifications are made to its motion system during its modeling process for the convenience of research: the outer ring of the bearing is fixed, the inner ring rotates around the Z-axis synchronously with the wheel axle of the vehicle, and the rollers are purely rolling on the raceway. The major parameters of the bearing model are shown in Table 1.

Table 1 Structural parameters of the bearings

Parameter	Value	Unit
Inner ring diameter (D_i)	130	mm
Outer ring diameter (D_o)	240	mm
Average roller of diameter (D)	26.5	mm
Number of single row rollers (N)	17	–
Effective length of rollers (l)	45	mm

In the modeling of the axle box bearing, its nonlinear contact force includes the contact force between the outer raceway and rollers (Q_o), the contact force between the inner raceway and rollers (Q_i), and the contact force between the inner ring flange and rollers (Q_f). α_i, α_o, and α_f are the contact angles, as shown in Fig. 2. According to the roller being in equilibrium, the equilibrium equation (1) can be listed as

$$\begin{cases} Q_\mathrm{o}\sin\alpha_\mathrm{o} - Q_\mathrm{i}\sin\alpha_\mathrm{i} - Q_\mathrm{f}\sin\alpha_\mathrm{f} = 0, \\ Q_\mathrm{o}\cos\alpha_\mathrm{o} - Q_\mathrm{i}\cos\alpha_\mathrm{i} - Q_\mathrm{f}\cos\alpha_\mathrm{f} = 0. \end{cases} \tag{1}$$

Take Q_o as the reference variable, and Eq. (1) can be transformed into the following forms:

$$Q_\mathrm{i} = Q_\mathrm{o}\frac{\sin(\alpha_\mathrm{o}+\alpha_\mathrm{f})}{\sin(\alpha_\mathrm{i}+\alpha_\mathrm{f})} = c_\mathrm{i}Q_\mathrm{o}, \quad Q_\mathrm{f} = Q_\mathrm{o}\frac{\sin(\alpha_\mathrm{o}-\alpha_\mathrm{f})}{\sin(\alpha_\mathrm{i}+\alpha_\mathrm{f})} = c_\mathrm{f}Q_\mathrm{o}. \tag{2}$$

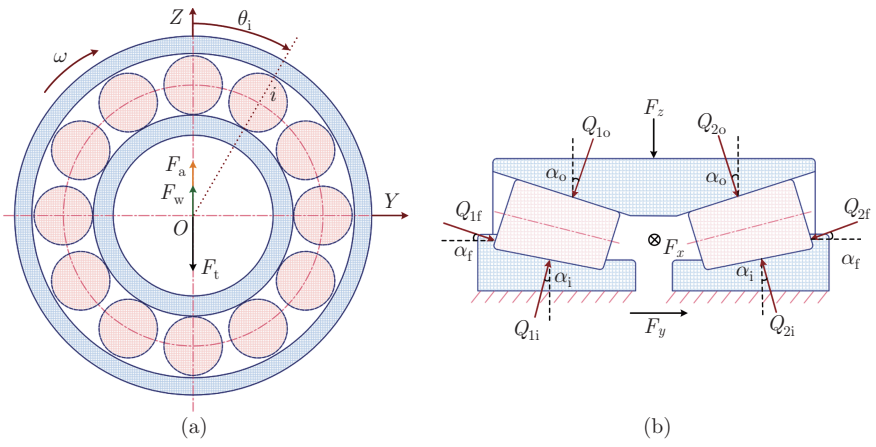

Fig. 2 Contact force of bearing (color online)

In addition, the Hertz contact theory can be used to infer the relationship between contact force and deformation. The roller's contact force is represented as follows:

$$Q_\mathrm{oi} = K_\mathrm{ne}\delta_\mathrm{ni}^{1.11}, \quad \delta_\mathrm{ni} > 0, \tag{3}$$

where δ_{ni} is the contact deformation of the outer raceway and rollers,

$$\delta_{\mathrm{ni}} = \delta_{ri} \cos\alpha_{\mathrm{o}} + \delta_{yi} \sin\alpha_{\mathrm{o}}, \tag{4}$$

where δ_{ri} represents the radial displacement of the outer ring relative to the inner ring, and δ_{yi} represents the displacement of the outer ring relative to the inner ring in the axial direction.

In addition, K_{ne} represents the total stiffness of the Hertz contact, it can be derived from the empirical formula for elastic deformation given by Palmgren[31],

$$K_{\mathrm{ne}} = \frac{3.84 \times 10^{-5}}{l^{0.8}} (1 + c_{\mathrm{i}}^{0.9} \cos(\alpha_{\mathrm{o}} - \alpha_{\mathrm{i}}))^{-1.11}. \tag{5}$$

By adding the contact loads of all the rollers, the total contact forces of the outer raceway in the X-, Y-, and Z-directions can be calculated as

$$F_{\mathrm{o}} = \sum_{m=1}^{2} \sum_{k=1}^{N} Q_{mok}. \tag{6}$$

Other contact forces such as Q_{i} and Q_{f} can be computed using Eq. (2) once Q_{o} has been solved. Similarly, F_{i} and F_{f} can be solved based on F_{o}.

If a local fault occurs in the bearing element, the roller passing through the defect will release some of the amount of deformation that it is compressed, marked as H_0, and Eq. (4) can be transformed into the following form:

$$\delta_{\mathrm{ni}} = \delta_{ri} \cos\alpha_{\mathrm{o}} + \delta_{yi} \sin\alpha_{\mathrm{o}} - \lambda H_0, \tag{7}$$

where λ takes 1 or 0 to indicate whether there is a non-linear Hertz contact force.

2.3 Model coupling and co-simulation

The forces between the bearing and the vehicle can interact to achieve coupling between the two models, and the connection between the two softwares is realized through the S-function module. Outputting the UM model to exchange data between the two models, and the co-simulation computation can be done in the MATLAB/SIMULINK. In the course of the co-simulation, the data of the vehicle model and the bearing model are exchanged, which are expressed as interaction forces between the vehicle and the axle box bearings. Among them, wheel-rail forces (F_{w}), primary suspension forces (F_{t}), and rotating arm node forces (F_{a}) act on the main components of the axle box bearings. The axle box bearings act on the axle box and wheelset of the vehicle through the non-linear forces (F_{o}, F_{i}, and F_{f}) generated by the Hertz contact. The co-simulation diagram is shown in Fig. 3. The detailed establishment processes of the bearing and bearing fault model, as well as the co-simulation between the vehicle and the bearing, have all been thoroughly and specifically described in Ref. [30].

3 Analysis of bearing vibration under track irregularity

The irregularity of the track during running of the vehicle can cause various vibrations in the vehicle system, which will inevitably have an effect on the axle box bearings. It is required to investigate bearing vibration under track irregularity conditions in order to conduct a more accurate and comprehensive analysis of the axle box bearings. Following the construction of the vehicle model, the rail vehicle/track/irregularities module can be used to simulate it by importing the track irregularities. In addition, wheel tread damage, such as wheel flats and wheel polygons, can be added to the created wheelset model using the rail vehicle/wheels/out-of-round module.

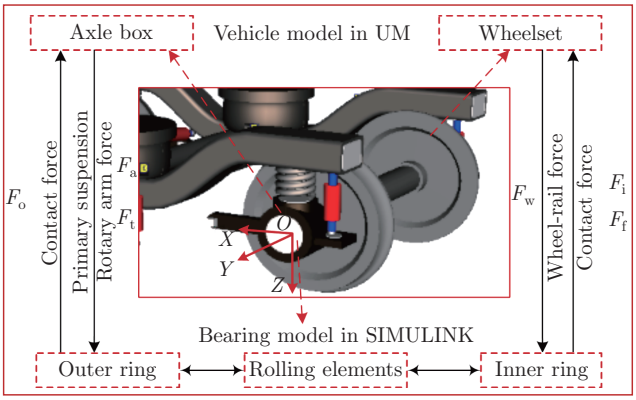

Fig. 3 Co-simulation diagram (color online)

3.1 Simulation analysis

The German high-interference track irregularity spectrum is used in the simulation because it has a well-established standard of use and can give a better response to the vibration characteristics of the axle box bearings in a shorter period of time. Set the vehicle speed to 300 km/h and simulate bearings with outer and inner ring faults, respectively. Figure 4 depicts the time domain of the lateral and vertical acceleration of the bearing, where WI (with irregularity) represents input track irregularity, and WOI (without irregularity) represents non-input track irregularity. The comparison between two working conditions reveals that under the influence of track irregularity, the bearing's acceleration fluctuates to varying degrees in the two directions. The maximum value of its acceleration, however, does not differ significantly with or without

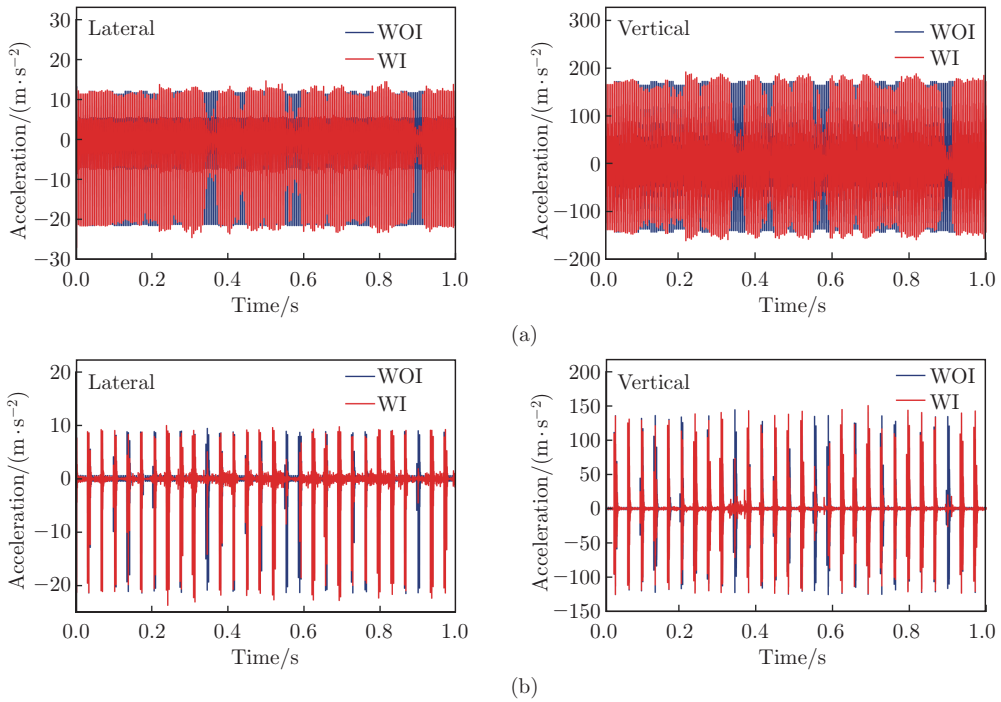

Fig. 4 Acceleration time domain diagram (simulation): (a) outer ring fault; (b) inner ring fault (color online)

track irregularities. This is due to the fact that the failure of the bearing components will result in a relatively large vibration acceleration of the bearing itself.

The bearing fault diagnosis algorithm based on resonance demodulation is a popular and widely used method for bearing fault detection. To further investigate the impact of track irregularity on signal characteristics, frequency domain features of acceleration signals in the lateral and vertical directions of bearings are extracted, and an envelope analysis is performed. The characteristic frequencies generated by bearing outer ring faults and inner ring faults can be calculated through the following equation:

$$f_{\mathrm{o}} = \frac{N}{2}\left(1 - \frac{D}{D_{\mathrm{m}}}\cos\alpha_{\mathrm{o}}\right) f_{\mathrm{s}}, \quad f_{\mathrm{i}} = \frac{N}{2}\left(1 + \frac{D}{D_{\mathrm{m}}}\cos\alpha_{\mathrm{o}}\right) f_{\mathrm{s}}, \tag{8}$$

where D is the diameter of the roller, D_{m} is the pitch diameter of the bearing, and f_{s} is the rotational frequency of the axle,

$$f_{\mathrm{s}} = \frac{V_0}{2\pi R}, \tag{9}$$

where V_0 is the running speed of the vehicle, and R is the radius of the wheel. The simulation results prove to be correct if the fault characteristic frequency of the bearing is extracted from the simulation results. The correctness of the simulation results can be further determined if they are close to the experimental results.

Set the speed to 300 km/h, Eqs. (8) and (9) can be utilized to calculate $f_{\mathrm{o}} = 210.5$ Hz, $f_{\mathrm{i}} = 279.64$ Hz, and $f_{\mathrm{s}} = 28.83$ Hz, respectively. The results for the outer ring fault bearing, as shown in Fig. 5, are consistent in both directions, and the track irregularity has no effect on the extraction of the outer ring fault characteristic frequency. The clear f_{o} and its multiples can still be detected under the assumption of inputting the track irregularity spectrum, but their

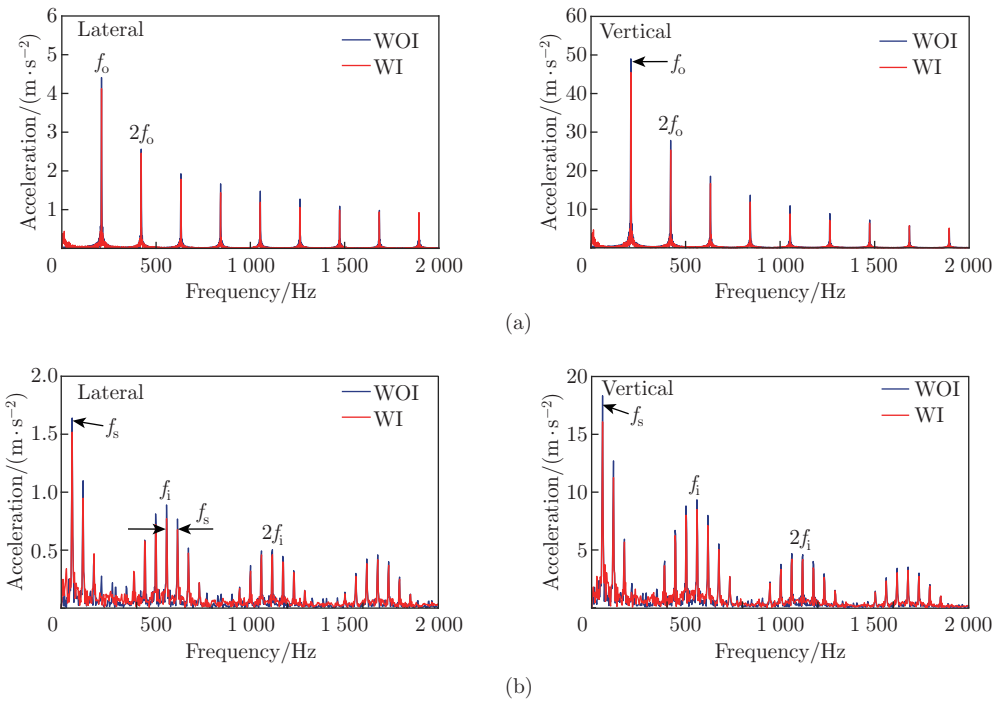

Fig. 5 Acceleration envelope spectrum (simulation): (a) outer ring fault; (b) inner ring fault (color online)

amplitude has decreased to some extent. For inner ring faulty bearings, as shown in Fig. 5, under the impact of track irregularity, f_s, f_i, and multiples of f_i can be detected. Sidebands exist on both sides of each inner ring fault characteristic frequency, separated by f_s. However, the amplitudes of f_s, f_i, and sidebands of f_i are somewhat reduced by the input track irregularity.

In summary, for faulty bearings, the fault characteristic frequencies can be detected in both the lateral and vertical directions, but it will reduce the amplitude of the spectrum to some extent, which is unfavorable for bearing fault detection based on resonance demodulation.

3.2 Experimental verification

The single wheelset rolling and vibrating test rig is a multi-use test bench that mimics the behavior of high-speed trains. Experiments are carried out on the rig to confirm the simulation's conclusion. Two axle box bearings are used in the experiment as the test subjects, and acceleration sensors are mounted on the east and west sides of the axle box. An outer ring fault bearing is installed on the east side of the axle box, and an inner ring fault bearing is installed on the other side. The inner/outer ring of the bearing has a wire-cut penetration wound with a width of 1 mm, which is a relatively serious outer ring fault. Assign a vertical load of 7 t, a running speed of 300 km/h, a sampling frequency of 25.6 kHz, and a sampling time of 60 seconds. Sensors at the upper end of the axle box end cover are used to gather the vertical and lateral acceleration signals of the axle box. The wheel rail excitation is set for two test conditions: input track irregularity and non-input track irregularity, and the vibration accelerations of the axle box bearing are collected. The experimental site is shown in Fig. 6.

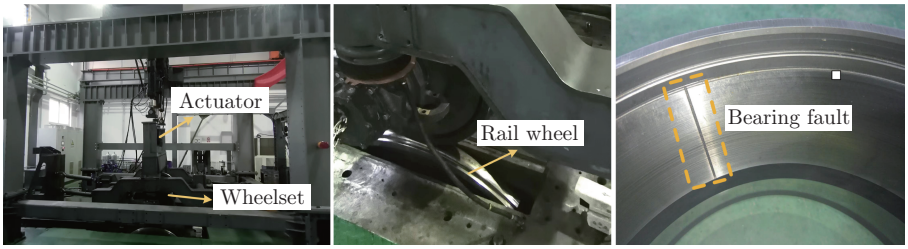

Fig. 6 Experimental site: (a) test rig; (b) arrangement of acceleration sensors; (c) bearing fault (color online)

Evaluate the time domain analysis of the extracted acceleration. Despite the presence of complex factors such as friction, noise, temperature, and lubrication in the experiment, the bearing's acceleration value remains large, particularly in the transverse direction, even in the absence of input track irregularity. The lateral and vertical acceleration of the bearing with the outer ring fault is shown in Fig. 7(a). There will be some fluctuations in the bearing's acceleration following the input track irregularity, but there is no significant difference. The track irregularity does not appear to have a significant impact on the acceleration of the outer ring fault bearing, which is consistent with the simulation results. Figure 7(b) depicts the lateral and vertical acceleration of the inner ring fault bearing. The shock effect caused by the inner ring fault is influenced by f_s because the faults revolve around the axle. The interval between the two impacts in the figure is exactly the axle rotation period, which agrees with the time-domain characteristics of the inner ring fault. Furthermore, the amplitude difference of the acceleration before and after input track irregularity is not significant, and it is in line with the outcomes of the simulation.

The acceleration envelope spectra with the outer ring fault are shown in Fig. 8(a). f_o and its multiples can be clearly detected after input track irregularity, but its amplitude decreases in degree. Figure 8(b) depicts the acceleration envelope spectrum with an inner ring fault. f_s, f_i and its multiplies, and the sidebands separated by f_s can all be detected after inputting the track

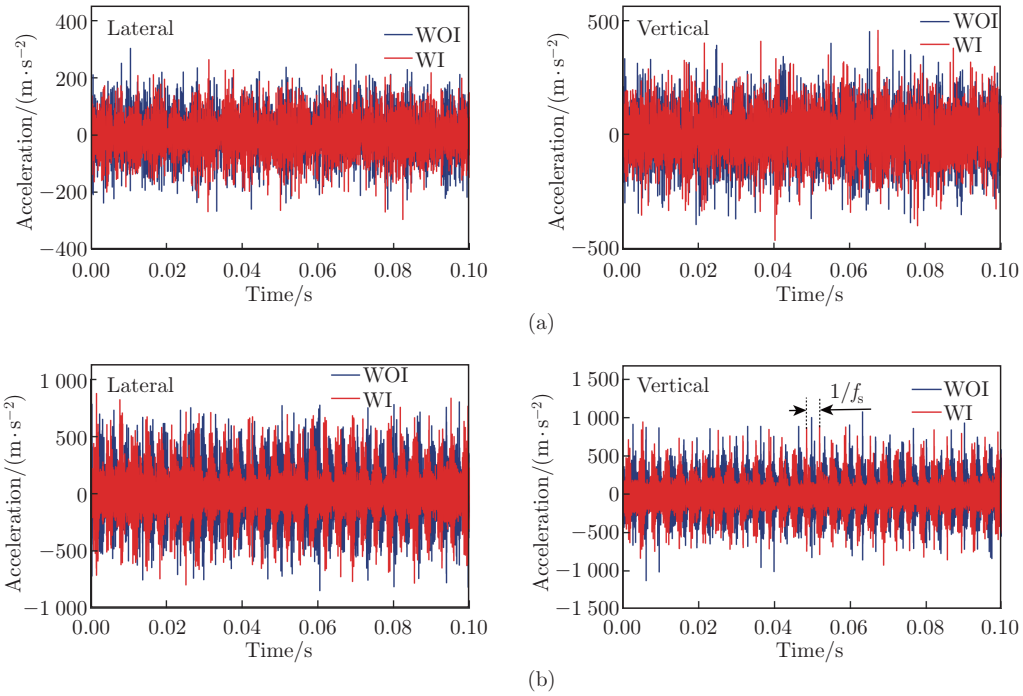

Fig. 7 Acceleration time domain diagram (experiment): (a) outer ring fault; (b) inner ring fault (color online)

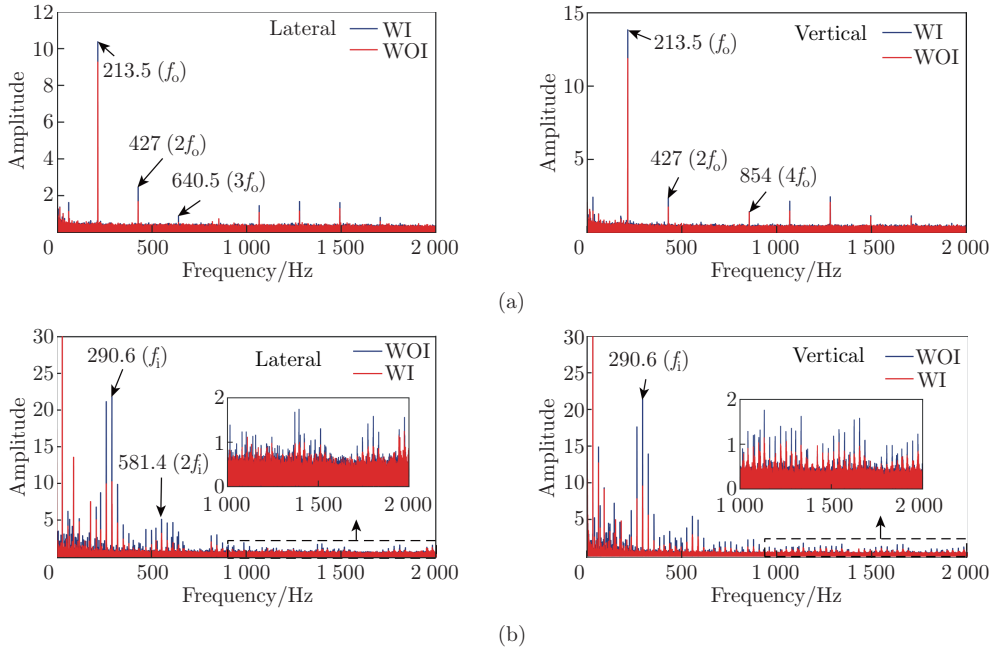

Fig. 8 Acceleration envelope spectrum (experiment): (a) outer ring fault; (b) inner ring fault (color online)

irregularity. The amplitude of the envelope spectrum, however, decreases under the influence of track irregularities. In summary, there is consistency between the results of the simulation and

the experiment, proving the correctness of the conclusions reached. That is, track irregularities will cause slight interference in fault detection and will weaken the component of fault frequency in the bearing signal to some extent. Concurrently, the strong agreement between simulation and experimental data confirms the accuracy of the established axle box bearing model.

4 Analysis of bearing vibration response to various wheel flat excitation

4.1 Wheel flat model

Wheel flats can be newly formed, transitional or rounded, which have varying depths at the start of their creation and fluctuate in length as they wear. The ideal newly formed wheel flat is a string line[32]. The margins of the wheel flat progressively smooth off to become a transitional one, which results in continuous impact and wear. With continued wear, a gradual increase in length is observed in the transition wheel flat, eventually forming the rounded wheel flat. The calculation of wheel flat size can be obtained by the following equations:

$$\begin{cases} L_0 = \sqrt{8Rd - d^2}, \\ Z(x) = (d/2)(1 + \cos(2\pi x/L_1)), \\ L_1 = \pi L_0/2, \end{cases} \tag{10}$$

where d is the depth of the newly formed flat, L_0 is its length, and L_1 is the rounded flat's minimum length that ensures the wheel's convex shape. The schematic diagram of the wheel flat is shown in Fig. 9. The wheel flat excitation will be manifested in the frequency domain as f_s. $Z(x)$ is the circumferential variation of the wheel radius, and x is the arc length along the surface tread of the wheel.

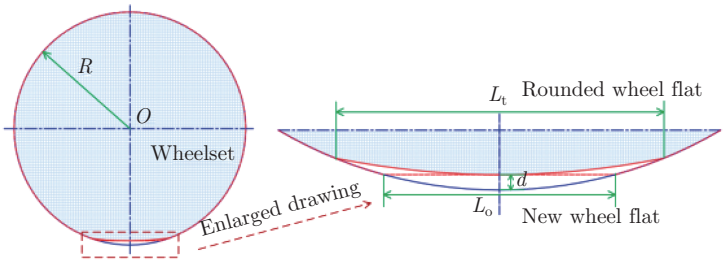

Fig. 9 Schematic diagram of wheel flat (color online)

4.2 Simulation and experimental verification

Set the simulation parameters to simulate normal and fault bearings, respectively, where the wheel flat depth is 0.1 mm, and the vehicle is running at 100 km/h. The time-frequency domain analysis of normal bearing acceleration in the vertical direction is shown in Fig. 10(a). The bearing acceleration exhibits obvious periodic vibration under excitation of wheel flat, and the time interval between the two vibrations is exactly the reciprocal of f_s. The frequency domain diagram clearly shows f_s and its multiplies. The time-frequency domain analysis of outer ring fault bearing is shown in Fig. 10(b). Two vibration impacts with different periods appear in the figure. The longer time interval between two impacts is the reciprocal of f_o, and the shorter time interval between two impacts is the reciprocal of f_s. The frequency domain reveals obvious f_o and its multiples, as well as f_s and its multiples. These vibration characteristics in both the time and frequency domains fully demonstrate the coupled model's correctness. Experiments will be performed to validate the simulation results.

In order to confirm the accuracy of the simulation results, experiments are conducted on the single wheelset rolling and vibrating test rig shown in Subsection 3.2. Due to the limited

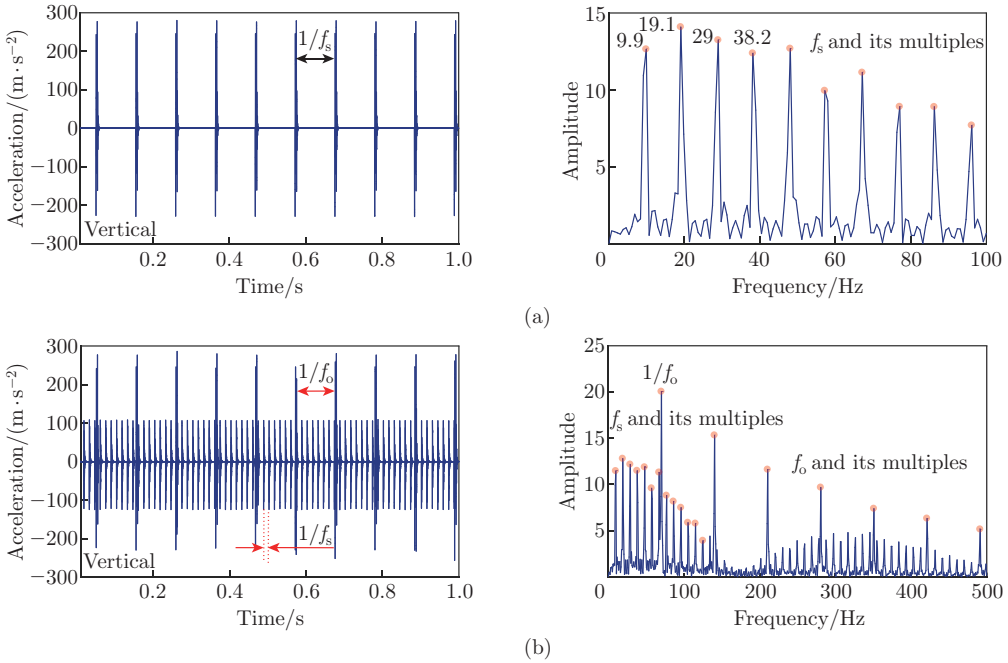

Fig. 10 Acceleration of bearing (simulation): (a) normal bearing; (b) outer ring fault bearing (color online)

experimental conditions, the wheel flat is placed on the tread of the east rail wheel with a depth of 40 µm. The fault size of the bearing is consistent with that of Subsection 3.2. Figure 11(a) depicts the normal bearing acceleration which exhibits obvious periodic vibration under the wheel flat excitation, and the time interval between the two vibrations is exactly the reciprocal of the rotation frequency of the rail wheel (f_w). f_w and its multiples can be observed on the frequency domain diagram. Figure 11(b) depicts the acceleration analysis of the outer ring fault bearing. Because of the influence of background noise in the system and the relatively small size of the rail wheel flat, no obvious vibration caused by the rail wheel excitation is detected in the time-domain, but obvious vibration caused by the bearing outer ring fault can be observed. Even though the amplitude is quite small, there are obvious f_o and its multiples as well as f_w and its multiples in the frequency domain.

This fully demonstrates that the calculation results obtained by the axle box bearing model in the vehicle and the wheel flat model established are reliable, and these models can be used for further simulation and analysis.

4.3 Simulation under different types of wheel flat

With the vehicle running at a speed of 100 km/h, the axle box bearing model is simulated independently under excitation of newly formed, transitional, and rounded wheel flats with a depth of 0.1 mm. Figure 12 reveals the bearing's acceleration in longitudinal, lateral, and vertical orientations. It can be found that in all the three circumstances, the vibration of the bearing is most affected and longest lasting by excitation of the newly formed wheel flat, which is followed by the transition wheel flat and the rounded wheel flat. This is because the angularity is more obvious when the wheel flat is first formed, which makes the instantaneous impact of the newly formed wheel flat on the bearing stronger. As transitional and rounded wheel flats have a smoother surface after wear, their impacts on the vibration of the bearing are less than those of a newly formed wheel flat. Because the lengths of the transitional wheel flat and rounded wheel flat increase with wear, the rounded wheel flat has the earliest influence on the bearing, followed by the transitional wheel flat and newly formed wheel flat.

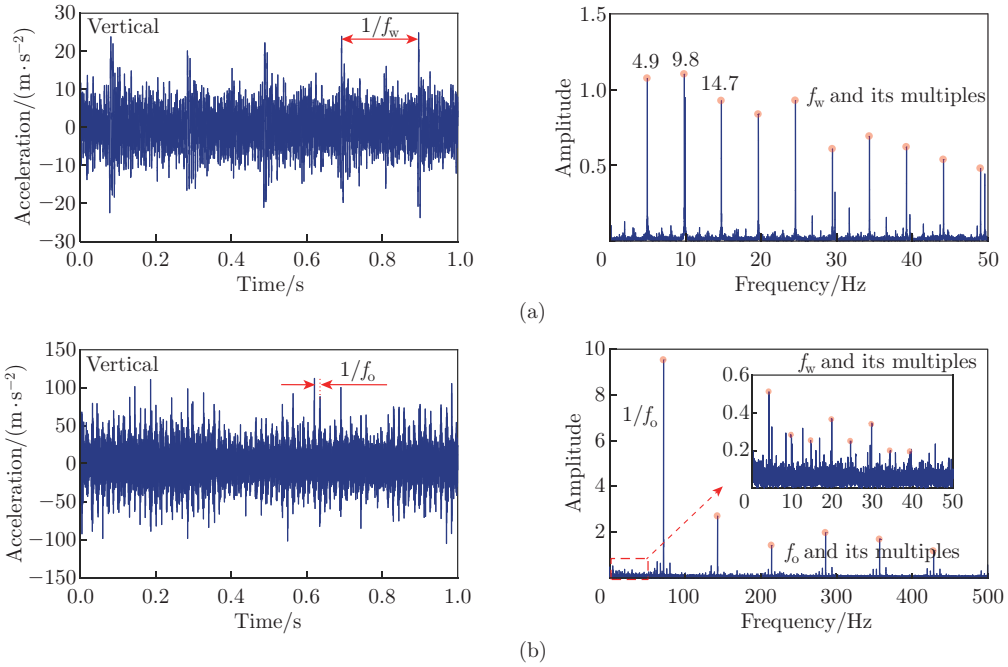

Fig. 11 Acceleration of bearing (experiment): (a) normal bearing in; (b) outer ring fault bearing (color online)

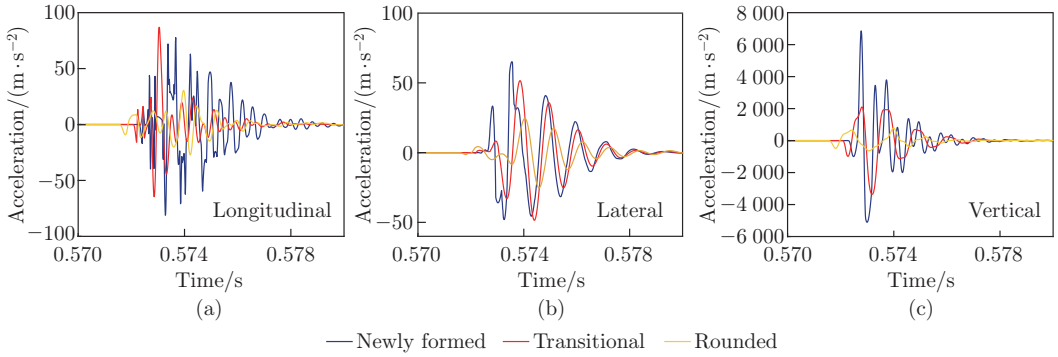

Fig. 12 Bearing accelerations: (a) longitudinal; (b) lateral; (c) vertical (color online)

As illustrated in Fig. 13(a), the longitudinal direction of vehicle operation is represented by the X-direction, the lateral direction of vehicle operation is represented by the Y-direction, and the vertical direction of vehicle operation is represented by the Z-direction. It shows that the root mean square (RMS) of its acceleration is the greatest in the vertical direction. The reason for this phenomenon is that the vertical direction is the direction in which the bearing is mainly loaded. Making use of the RMS of the bearing's acceleration under the impact of the rounded wheel flat as a reference, the RMS graphs of the bearing's acceleration corresponding to excitation of the newly formed and the transitional wheel flats are compared, respectively, as shown in Fig. 13(b). It can be found that, the RMS under excitation of the newly formed wheel flat can reach 5.47 times that of the rounded wheel flat in vertical. Besides, the impact under the transitional wheel flat is 2.53 times greater than that under the rounded wheel flat. In the longitudinal direction, the RMS under the impact of the newly formed wheel flat is 2.04

times greater than that under the rounded wheel flat, and the RMS under the impact of the transitional wheel flat is 1.58 times greater than that under the rounded wheel flat. As a result, when the wheel flat first forms, the bearing vertical acceleration is extremely great, followed by lateral and longitudinal accelerations. The acceleration gradually decreases with the wear of wheel flats.

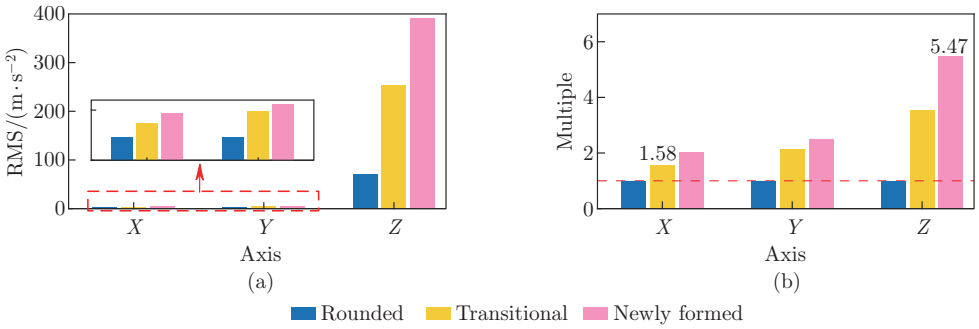

Fig. 13 The RMS of the bearing's acceleration: (a) values in three directions; (b) multiple (color online)

As shown in Fig. 14, changes in the vehicle's running speed can alter the interaction between the wheel and track, affecting the vibration of the bearing. The RMSs of the bearing's accelerations vary with speeds under excitation of three types of wheel flats, and in the longitudinal direction, the RMSs under the excitation of the three types of wheel flats are relatively similar. All of them show a gradually increasing trend, with the rate of increase being faster under excitation of the rounded wheel flat and eventually surpassing those under the newly formed and transitional wheel flats. In the lateral direction, the RMSs increase and then decrease and gradually stabilize under the excitation of all three types of wheel flats, with the RMS of the acceleration under excitation of the newly formed wheel flat peaking at about 60 km/h, that under excitation of the transition wheel flat peaking at about 90 km/h, and that under the excitation of the rounded wheel flat peaking at about 120 km/h. It can be found that as the length of the wheel flat increases, so does the vehicle speed corresponding to the peak point of the RMS. In the vertical direction, the RMS of the acceleration increases gradually in all three cases, and at a speed of about 240 km/h, the RMS under excitation of the transitional wheel flat exceeds that under the newly formed wheel flat. Overall, the newly formed wheel flat has a greater impact on the bearing in the vertical and lateral directions. But the importance of the rounded wheel flat cannot be ignored, because in the longitudinal direction, its influence

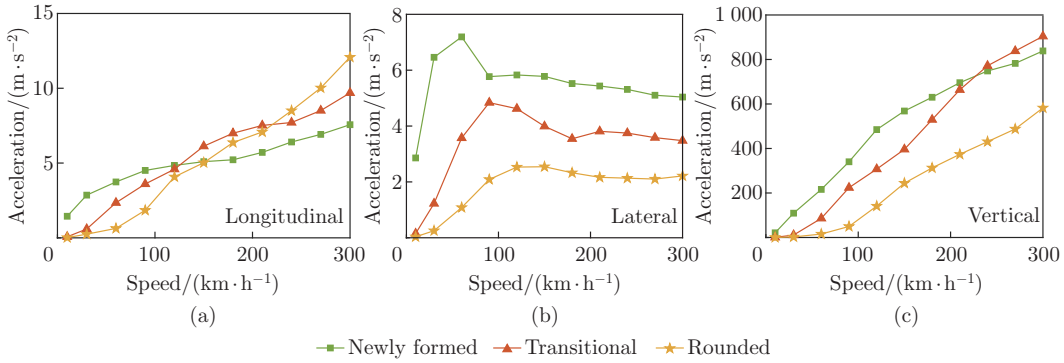

Fig. 14 The RMS of bearing's acceleration: (a) longitudinal; (b) lateral; (c) vertical (color online)

on the bearing will gradually increase with the vehicle speed and outweigh that of the newly formed and transitional wheel flats.

4.4 Simulation of changes in the length of the rounded wheel flat

The vehicle speed and wheel flat size are critical factors in studying the effect of wheel flat impact. Newly formed wheel flat forms and wears out quickly as vehicle mileage increases and the wheel rotates at high speeds, so rounded wheel flat is a common form. During gradual wear, the wheel flat remains constant in depth and gradually increases in length, and this change may affect the vibration of the bearing in varying degrees. Set the conditions as follows: the depth of the rounded wheel flat is 0.1 mm, and the length varies from 40 mm to 100 mm, the acceleration peak of the bearing is shown in Fig. 15. The change in length represents the gradual wear of the wheel flat. As shown Fig. 15, the length of the wheel flat is constant, and acceleration peaks of the bearing in the vertical and longitudinal directions will increase continuously as speed increases. Acceleration peaks in the lateral direction increase first and then decrease. From the overall view, at the same vehicle speed, vibrations in three directions follow the following trend: the longer the wheel flat is, the smaller the acceleration peak of the bearing is. This is because the wheel flat wears to make the curvature of the wheel more rounded and smoother, reducing the impact on the track and the vibration shock transmitted to the bearings.

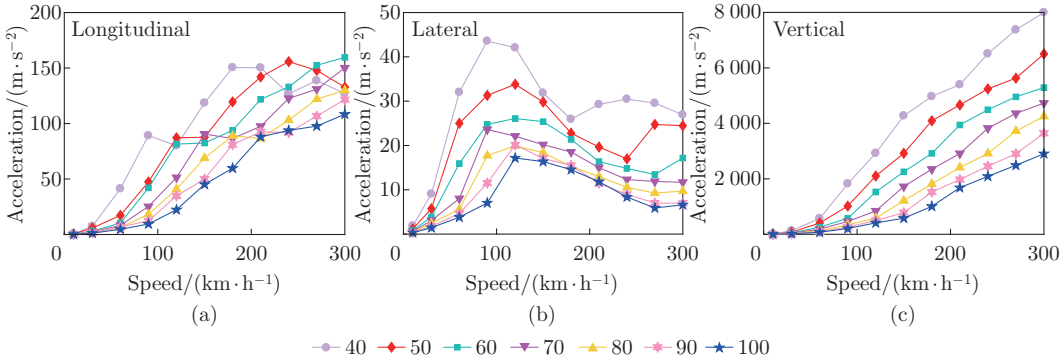

Fig. 15 Bearing's acceleration peak: (a) longitudinal; (b) lateral; (c) vertical (color online)

Simulation results are taken for vehicle speeds of 30 km/h, 150 km/h, and 300 km/h. The three speeds represent the low, medium, and high speeds of the vehicle, respectively. Define an indicator, the variation index "V_{I}". It represents the variation of the bearing's acceleration peak under excitation of the rounded wheel flat, and it can be obtained through dividing the acceleration peak under excitation of the transition wheel flat by the acceleration peak under excitation of different wheel flat lengths. According to Fig. 16, in the longitudinal direction, V_{I} gradually rises along with the increase in the flat length at the low vehicle speed. The variations fluctuate at the medium and high speeds, and a positive increase occurs at the high speed. Overall, the variation of the acceleration peak at low speed is greatest, followed by that at medium speed, and then at high speed. In the lateral direction, V_{I} increases as the length of the flat increases at different vehicle speeds. The variation of the acceleration peak at low speed is the greatest, followed by that at high speed and medium speed. In the vertical direction, with the increase in the flat length, V_{I} at different velocities gradually increases. The conclusion at speed condition is the same as in the longitudinal direction.

As a result, V_{I} is greater when the length is longer, and the vehicle speed is lower under the condition when the depth of the flat is constant. Therefore, when the wheel has a flat defect after a longer period of wear, the bearing is more likely to be damaged during low-speed operation.

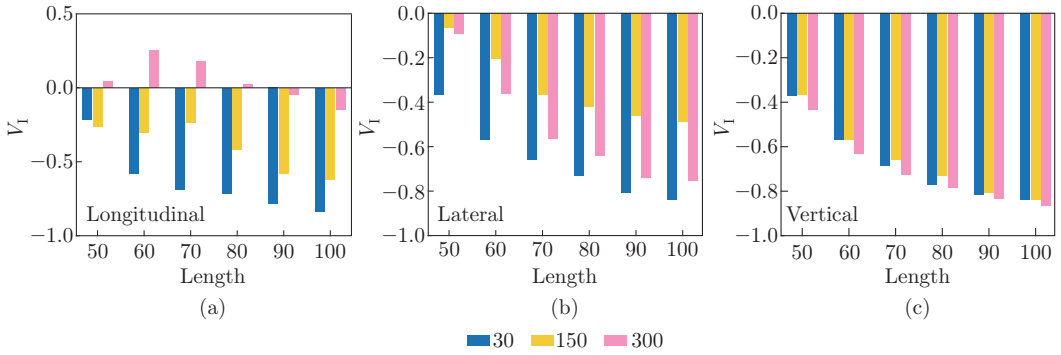

Fig. 16 Variation index of the acceleration peak: (a) longitudinal; (b) lateral; (c) vertical (color online)

4.5 Simulation of changes in the depth of the rounded wheel flat

Wheel flats are a type of tread scuffing that may form at different depths as the wheel rotates, causing different effects on the vibration of the bearing. Set the conditions as follows: the length of the flat is 80 mm, and the depth varies in the range of 0.1 mm to 0.6 mm, the acceleration peak of the bearing under excitation of the rounded wheel flat is shown in Fig. 17. It can be found that when the depth of the flat is constant, the acceleration peaks in the vertical and longitudinal directions increase gradually with the vehicle speeds, while the peak in the lateral direction increases and then decreases. When the vehicle speed and the length of the flat are constants, acceleration peaks in all three directions increase gradually as the depth of the flat increases.

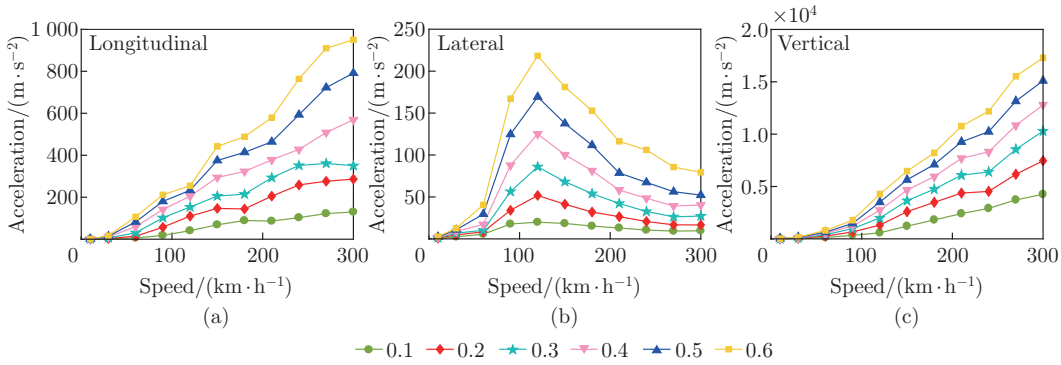

Fig. 17 Bearing's acceleration peak: (a) longitudinal; (b) lateral; (c) vertical (color online)

Simulation results are obtained under the conditions when the vehicle speeds are 30 km/h, 150 km/h, and 300 km/h, respectively. To get V_I in three directions, the acceleration peak of the bearing under excitation of different wheel flat depths is divided by the acceleration peak under excitation of 0.1 mm depth, respectively. According to Fig. 18, when the vehicle has a stable speed in the longitudinal direction, V_I steadily increases with the increase in the flat depth. Overall, the variation of the acceleration peak at low speed is the greatest, followed by that at the high speed, and then at the medium speed. In the lateral direction, V_I gradually increases with the increase in the flat depth. The variation of the acceleration peak at the medium speed is the greatest, followed by that at the high speed, and then at the low speed. V_I is gradually rising in the vertical direction along with the increase in the flat depth. The variation of the acceleration peak grows more quickly at the low speed, followed by the medium speed, and then at the high speed.

Therefore, if the depth of the flat is greater, the variations of the peaks in the vertical and longitudinal directions are larger at the low speed, and the variation of the peak in the lateral direction is larger at the medium speed. As a result, when there is a deep flat on the wheel, the vehicle's low and medium speed operation will cause more damage to the axle box bearings and may cause them damage.

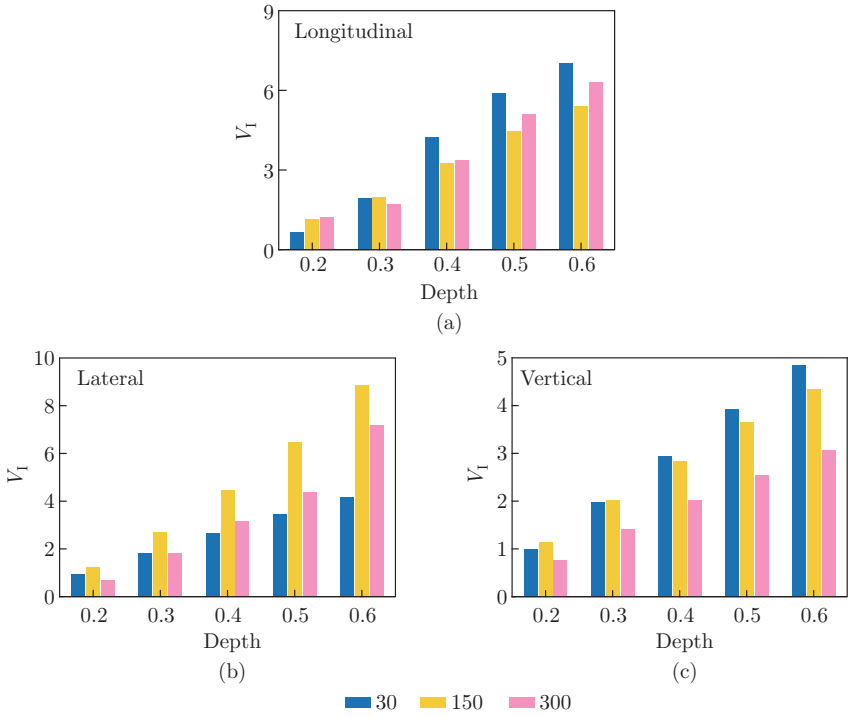

Fig. 18 Variation index of the acceleration peak: (a) longitudinal; (b) lateral; (c) vertical (color online)

5 Vibration contributions of wheel flat and track irregularity

The track irregularity and the wheel flat will cause strong wheel-rail excitation, which will have an effect on the vibration of the axle box bearing, so the bearing vibrations under the two excitation are analyzed to investigate their contributions. The size of the wheel flat is selected as input to be 0.1 mm deep. Based on test results, Liu et al.[33] estimated the vibration contributions of different types of excitation to the amplitude characteristics of the axle box and gearbox. By calculating the difference of acceleration amplitude, the amplitude components of each excitation can be separated approximately. A similar approach is used in this paper to investigate the contribution of track irregularity and wheel flat excitation to the amplitude characteristics of axle box bearing vibration acceleration. As shown in Fig. 19, TI represents the track regularity, and WF represents the wheel flat. The vehicle speed of 150 km/h is selected as an example. In the longitudinal direction, the amplitude components of the bearing caused by the wheel flat excitation and track irregularity are 70.75 m/s^2 and 3.98 m/s^2, respectively, with a composition ratio of 94% and 6%. In the lateral direction, the contributing magnitudes are 18.68 m/s^2 and 0.71 m/s^2, respectively, with a composition ratio of 96% and 4%. In the vertical direction, the contributing magnitudes are 630.42 m/s^2 and 15.78 m/s^2, respectively, with a composition ratio of 98% and 2%. It is obvious that the vibration of the bearing caused by wheel flats is much greater than that caused by track irregularity. The wheel flat will generate

periodic worse shocks to the bearings, which can be fatal to the health of the bearings, so it is essential to study the vibration characteristics of axle box bearings under excitation of the wheel flat.

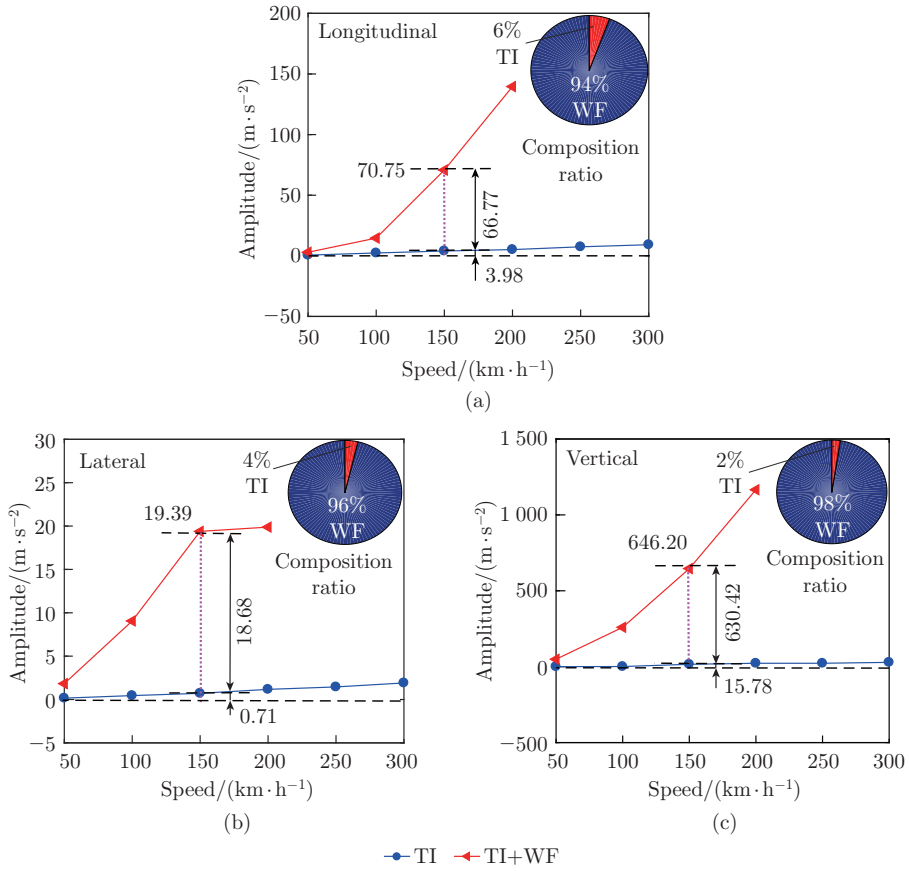

Fig. 19 Acceleration amplitudes of (a) longitudinal; (b) lateral; (c) vertical (color online)

In addition, the contribution of track irregularity and wheel flat excitation to the amplitude characteristics of internal contact force of the axle box bearing is analyzed, as shown in Fig. 20. At the speed of 150 km/h, the amplitude components of the the contact force caused by the wheel flat excitation and track irregularity are 1 037 N and 3 946 N in the longitudinal direction, respectively, with a composition ratio of 21 % and 79 %. In the lateral direction, the contributing magnitudes are 699 N and 740 N, respectively, with a composition ratio of 49 % and 51 %. In the vertical direction, the contributing magnitudes are 12 406 N and 89 060 N, respectively, with a composition ratio of 12 % and 88%. It can be found that at this speed, the bearing contact force is more affected by the track irregularity than the wheel flat excitation. But on the whole, with the increase in speed, the contribution of the wheel flat excitation to the bearing contact force amplitude gradually increases, which further illustrates the importance of wheel flat excitation on the bearing vibration.

6 Conclusions

An axle box bearing model included in the vehicle is used in the paper to study the dynamic response of axle box bearings under wheel-rail excitation. The correctness of the model and

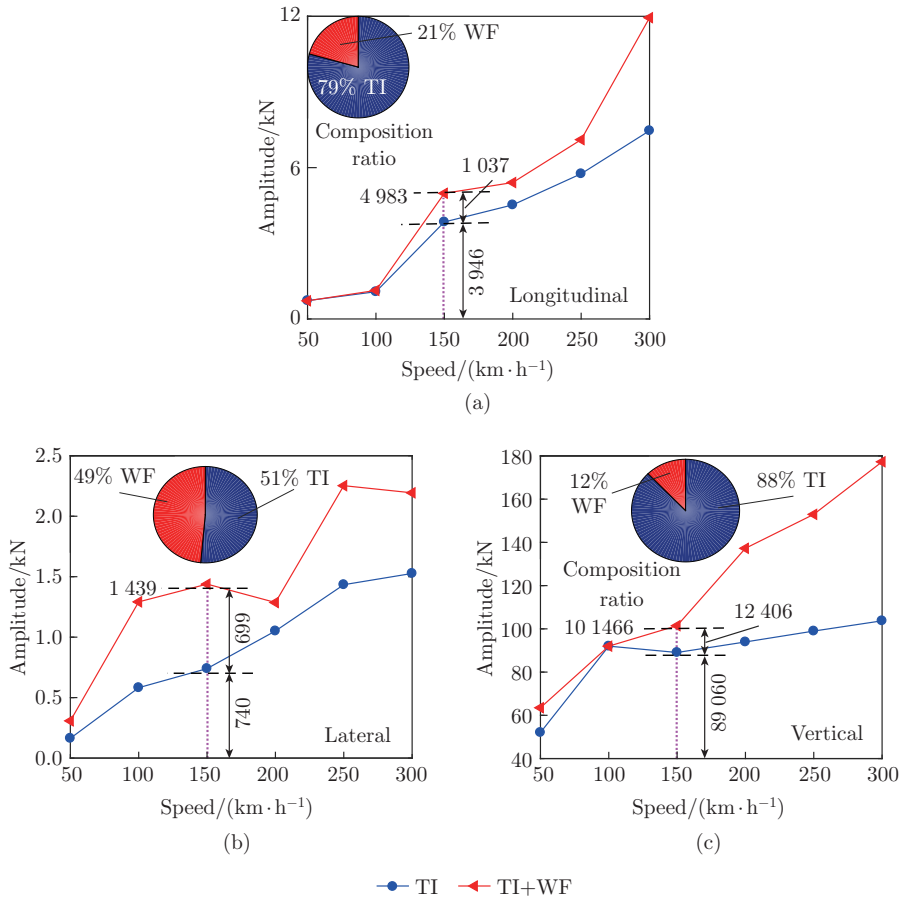

Fig. 20 Contact force amplitudes of (a) longitudinal; (b) lateral; (c) vertical (color online)

some conclusions is verified through simulation and experiments. The findings of the study are summarized as follows.

(i) Under excitation of track irregularity, the bearing's acceleration does not differ significantly in time domain. Track irregularities have slight interference in fault detection, weaken the component of fault frequency in the bearing signal to some extent, and reduce the amplitude of the spectrum, which is unfavorable for bearing fault detection based on resonance demodulation.

(ii) Excitation of the newly formed wheel flat has the greatest magnitude and duration of impact on the vibration of the bearing, followed by the transition wheel flat and the rounded wheel flat. The impact gradually decreases as the wheel flats wear. As the vehicle speed increases, the effect of the rounded wheel flat on the vibration of the bearing cannot be understated in the longitudinal direction.

(iii) At the same vehicle speed, the peak acceleration of the bearing is inversely proportional to the length of the flat and directly proportional to its depth. When the depth of the flat is constant, longer length and low vehicle speed will lead to a greater V_{I} on the acceleration of the bearing. When the length of the flat is certain, greater depth and low or medium vehicle speed will lead to a greater V_{I} on the acceleration of the bearing, both of which may cause a greater probability of bearing damage.

(iv) The vibration amplitude of bearing acceleration caused by wheel flat excitation is extremely large compared with that caused by track irregularities. At the same speed, the track

irregularity has a relatively larger impact on the bearing contact force. As speed increases, the effect of wheel flat excitation on bearings should be paid more attention.

Conflict of interest The authors declare no conflict of interest.

Acknowledgements The present work is supported by the National Scholarship Council of China.

References

[1] XU, L. and YU, Z. W. Dynamic solution for vehicle-track interaction considering the elastoplasticity of track slabs. *Journal of Vibration and Control*, **27**(13-14), 1668–1680 (2021)

[2] LIANG, B., LUO, H., and MA, X. N. Dynamic model of vertical vehicle-subgrade coupled system under secondary suspension. *Applied Mathematics and Mechanics* (*English Eidtion*), **28**(6), 769–778 (2007) https://doi.org/10.1007/s10483-007-0607-z

[3] YIN, S. C., PENG, T., YANG, C., YANG, C, H., CHEN, Z. W., and GUI, W. H. Dynamic hybrid observer-based early slipping fault detection for high-speed train wheelsets. *Control Engineering Practice*, **142**, 105736 (2024)

[4] HAN, L. L., JING, L., and LIU, K. A dynamic simulation of the wheel-rail impact caused by a wheel flat using a 3-D rolling contact model. *Journal of Modern Transportation*, **25**, 124–131 (2017)

[5] HAN, L. L, JING, L., and ZHAO, L. Finite element analysis of the wheel-rail impact behavior induced by a wheel flat for high-speed trains: the influence of strain rate. *Proceedings of the Institution of Mechanical Engineers*, *Part F*: *Journal of Rail and Rapid Transit*, **232**(4), 990–1004 (2018)

[6] JING, L. and HAN, L. L. Further study on the wheel-rail impact response induced by a single wheel flat: the coupling effect of strain rate and thermal stress. *Vehicle System Dynamics*, **55**(12), 1946–1972 (2017)

[7] STEENBERGEN, M. J. The role of the contact geometry in wheel-rail impact due to wheel flats. *Vehicle System Dynamics*, **45**(12), 1097–1116 (2007)

[8] LIU, Y., LIU, J. X., and GUO, Y. J. Study on dynamic simulation input form of locomotive wheel flat. *Applied Mechanics and Materials*, **215**, 946–949 (2012)

[9] BIAN, J., GU, Y. T., and MURAAY, M. H. A dynamic wheel-rail impact analysis of railway track under wheel flat by finite element analysis. *Vehicle System Dynamics*, **51**, 784–797 (2013)

[10] BIAN, J., GU, Y. T., and MURAAY, M. H. Numerical study of impact forces on railway sleepers under wheel flat. *Advances in Structural Engineering*, **16**(1), 127–134 (2013)

[11] QIN, Y. D., HU, M., YANG, L. Q., and ZHOU, X. Mechanics characteristics analysis of wheel/rail impact induced by wheel flats based on SIMPACK. *China Mechanical Engineering*, **28**(17), 2029 (2017)

[12] DUKKIPATI, R. V. and DONG, R. G. Impact loads due to wheel flats and shells. *Vehicle System Dynamics*, **31**, 1–22 (1999)

[13] ZHAO, D., HONG, J., YAN, K., ZHAO, Q. Q., and FANG, B. Dynamic interaction between the rolling element and cage of rolling bearing considering cage flexibility and clearance. *Mechanism and Machine Theory*, **174**, 104905 (2022)

[14] LU, Z. G., WANG, X. C., YUE, K. Y., WEI, J. Y., and ZHE, Y. Coupling model and vibration simulations of railway vehicles and running gear bearings with multitype defects. *Mechanism and Machine Theory*, **157**, 104215 (2021)

[15] LI, C. F., ZHOU, S. H., LIU, J., and WEN, B. C. Coupled lateral-torsional-axial vibrations of a helical gear-rotor-bearing system. *Acta Mechanica Sinica*, **30**(5), 746–761 (2014)

[16] LIU, J. and SHAO, Y. Vibration modelling of nonuniform surface waviness in a lubricated roller bearing. *Journal of Vibration and Control*, **23**(7), 1115–1132 (2017)

[17] LIU, J. and SHAO, Y. An improved analytical model for a lubricated roller bearing including a localized defect with different edge shapes. *Journal of Vibration and Control*, **24**(17), 3894–3907 (2018)

[18] WANG, B. S., LIU, Y. Q., and ZHANG, B. Characteristics analysis on bearing roter sysytem of high-speed train under variable conditions. *Chinese Journal of Theoretical and Applied Mechanics*, **54**, 1839–1852 (2022)

[19] LIU, Y. Q., WANG, B. S., YANG, S. P., LIAO, Y. Y., and GUO, T. Characteristics analysis of mechanical thermal coupling model of bearing rotor system of high-speed train. *Applied Mathematics and Mechanics* (*English Eidtion*), **43**(9), 1381–1398 (2022) https://doi.org/10.1007/s10483-022-2893-5

[20] TIAN, J., AI, Y. T., FEI, C. W., ZHANG, F. L., and CHOY, Y. S. Dynamic modeling and simulation of inter-shaft bearings with localized defects excited by time-varying displacement. *Journal of Vibration and Control*, **25**(8), 1436–1446 (2019)

[21] HOU, Y., WANG, X., QUE, H. B., GUO, R. B., LIN, X. H., JIN, S. Q., WU, C. P., ZOU, Y., and LIU, X. L. Variation in contact load at the most loaded position of the outer raceway of a bearing in high-speed train gearbox. *Acta Mechanica Sinica*, **37**, 1683–1695 (2021)

[22] LIU, Y. Q., CHEN, Z. G., WANG, K. Y., and ZHAI, W. M. Dynamic modelling of traction motor bearings in locomotive-track spatially coupled dynamics system. *Vehicle System Dynamics*, **60**(8), 2686–2715 (2022)

[23] LIU, Y. Q., CHEN, Z. G., LI, W., and WANG, K. Y. Dynamic analysis of traction motor in a locomotive considering surface waviness on races of a motor bearing. *Railway Engineering Science*, **29**, 379–393 (2021)

[24] LI, T., SUN, W., MENG, Z. C., HUO, J. Z., DONG, J. H., and WANG, L. P. Dynamic investigation on railway vehicle considering the dynamic effect from the axle box bearings. *Advances in Mechanical Engineering*, **11**(4), 1–13 (2019)

[25] LIU, J., LI, X. B., and YU, W. N. Vibration analysis of the axle bearings considering the combined errors for a high-speed train. *Proceedings of the Institution of Mechanical Engineers*, *Part K*: *Journal of Multi-Body Dynamics*, **234**(3), 481–497 (2020)

[26] WANG, Z. W., SONG, Y., YIN, Z. H, WANG, R. C., and ZHANG, W. H. Random response analysis of axle-box bearing of a high-speed train excited by crosswinds and track irregularities. *IEEE Transactions on Vehicular Technology*, **68**(11), 10607–10617 (2019)

[27] WANG, T. T., WANG, Z. W., SONG, D. L., ZHANG, W. H., LI, J. Y., and CHEN, D. Effect of track irregularities of high-speed railways on the thermal characteristics of the traction motor bearing. *Proceedings of the Institution of Mechanical Engineers*, *Part F*: *Journal of Rail and Rapid Transit*, **235**(1), 22–34 (2021)

[28] CHENG, L. Z., LIU, D. K., WANG, Y., and CHEN, A. Q. Load distribution and contact of axle box bearings in electric multiple units. *International Journal of Simulation Modelling*, **18**(2), 290–301 (2019)

[29] MA, Z. M., ZHU, H., CAO, Y. B., and YANG, S. P. Evolution of microstructure and mechanical properties of the high-speed train bearing under different service periods. *Materials Science and Engineering*, **800**, 140345 (2021)

[30] MA, Q. Y., LIU, Y. Q., YANG, S. P., and WANG, B. S. A coupling model of high-speed train-axle box bearing and the vibration characteristics of bearing with defects under wheel rail excitation. *Machines*, **10**, 1024 (2022)

[31] PALMGREN, A. *Ball and Roller Bearing Engineering*, SKF Industries Inc., Philadelphia (1959)

[32] ZHAI, W. M. Dynamic effect of wheel flats in railway. *Roll Stock*, **7**, 1–5 (1994)

[33] LIU, P. F., YANG, S. P., and LIU, Y. Q. Full-scale test and numerical simulation of wheelset-gear box vibration excited by wheel polygon wear and track irregularity. *Mechanical Systems and Signal Processing*, **167**, 108515 (2022)